UC Berkeley

Title

Simultaneous Imaging of Ga-DOTA-TATE and Lu-DOTA-TATE in Murine Models of Neuroblastoma

Permalink

https://escholarship.org/uc/item/7c58x58d

Journal

ISSN

Authors

Zheng, Yifan
Huh, Yoonsuk
Vetter, Kai
et al.

Publication Date

2023

DOI

Peer reviewed

Simultaneous Imaging of Ga-DOTA-TATE and Lu-DOTA-TATE in Murine Models of Neuroblastoma

Yifan Zheng,
Department of Nuclear Engineering, University of California, Berkeley, CA 94720, USA

Yoonsuk Huh,
Department of Radiology and Biomedical Imaging, University of California, San Francisco, CA 94143, USA.

Kai Vetter,
Department of Pediatrics, University of California, San Francisco, CA 94143, USA.

Nicole Nasholm,
Department of Pediatrics, University of California, San Francisco, CA 94143, USA.

Clay Gustafson,
Department of Pediatrics, University of California, San Francisco, CA 94143, USA.

Youngho Seo
Department of Radiology and Biomedical Imaging, University of California, San Francisco, CA 94143, USA, and with Department of Nuclear Engineering, University of California, Berkeley, CA 94720, USA.

Abstract

^{68}Ga-DOTA-TATE and ^{177}Lu-DOTA-TATE are radiolabeled somatostatin analogs used to detect or treat neuroendocrine tumors. They are administered separately for either diagnostic or therapeutic purposes but little experimental data for their biokinetics are measured simultaneously in the same biological model. By co-administering ^{68}Ga-DOTA-TATE and ^{177}Lu-DOTA-TATE in three laboratory mice bearing two IMR32 tumor xenografts expressing different levels of somatostatin receptors (SSTRs) on their shoulders and imaging both ^{68}Ga and ^{177}Lu simultaneously, we investigated the relationship between the uptake of ^{68}Ga-DOTA-TATE and ^{177}Lu-DOTA-TATE in organs and tumors. In addition, using the percent of injected activity (%IA) values of ^{68}Ga-DOTA-TATE at 0 hr and 4 hr, we investigated the correlation between ^{68}Ga-DOTA-TATE %IA and the time-integrated activity coefficients (TIACs) of ^{177}Lu-DOTA-TATE to estimate the organ-based and tumor-based doses of ^{177}Lu-DOTA-TATE. The results showed that the extrapolated clearance time of ^{68}Ga-DOTA-TATE linearly correlated with the TIACs of ^{177}Lu-DOTA-TATE in the IMR32-SSTR2 tumor, kidneys, brain, heart, liver, stomach and remainder body. The extrapolated %IA value at 0 hr of ^{68}Ga-DOTA-TATE linearly correlated with the TIACs of ^{177}Lu-DOTA-TATE in the IMR32 tumor and lungs. In our murine study, both kidneys and lungs were organs that showed high absorbed doses of ^{177}Lu-DOTA-TATE.

yifanzheng@berkeley.edu .

Keywords

^{68}Ga-DOTA-TATE; ^{177}Lu-DOTA-TATE; IMR32; neuroendocrine tumor; neuroblastoma; somatostatin receptor; SSTR; radiation dosimetry

---

I. INTRODUCTION

WITH the increasing trend of incidence of neuroendocrine tumors (NETs) [1], there is an increasing demand for the diagnosis and treatment of NETs [2]. Neuroblastoma is a type of NETs, and is most commonly found in young children [3]. Since somatostatin receptors (SSTRs) are shown to be highly expressed in NETs [4], NETs could be imaged and treated with SSTR-targeted agents. ^{68}Ga-labeled dodecane tetraacetic acid tyrosine-3-octreotate (^{68}Ga-DOTA-TATE) and ^{177}Lu-labeled DOTA-TATE (^{177}Lu-DOTA-TATE) are a theranostic pair of radiolabeled somatostatin analogs with high affinity specifically to SSTR type 2 (SSTR2). They are used to detect NETs by functional imaging techniques, like PET/CT for ^{68}Ga-DOTA-TATE and SPECT/CT for ^{177}LuDOTA-TATE [4]. Given that ^{68}Ga has a half-life of 67.71 minutes and goes through electron capture and β^+ decay, it is commonly used for imaging and diagnosis. In comparison, ^{177}Lu has a longer half-life (6.647 days) and goes through β^- decay, emitting low intensity gamma rays (The branching ratios are 10.41% for 208 keV gamma rays and 6.23% for 113 keV gamma rays) as well as therapeutic β-particles. Based on that, ^{177}Lu is not preferred for diagnostic imaging because of the suboptimal imaging characteristics but mainly used for targeted radiotherapy [5]. Since ^{68}Ga-DOTA-TATE and ^{177}Lu-DOTA-TATE are structurally similar but not identical, we were interested in investigating the *in vivo* biokinetics of ^{68}Ga-DOTA-TATE and ^{177}Lu-DOTA-TATE in organs and tumors simultaneously when they are administered at the same time.

When possible, pretherapy dosimetry to estimate the absorbed dose in tumors and normal organs helps better guide the patient-specific therapy [5], [6]. For example, PET/CT imaging of ^{124}I could be used to estimate the organ-based absorbed dose of ^{131}I radiotherapy by utilizing the pretherapy ^{124}I-based imaging data [5], [7]. The mean standardized uptake values (SUVs) of ^{68}Ga-DOTATOC or ^{68}Ga-DOTA-TATE in PET/CT images were also found to be linearly correlated with the absorbed dose of ^{177}Lu-DOTA-TATE in tumors and critical organs including kidneys, liver, and bone marrow, which could then be used to predict the absorbed dose of ^{177}Lu-DOTA-TATE in tumors and critical organs [8], [9]. It also showed that with only one ^{68}Ga-PSMA-11 PET scan at 1 hr postinjection, the absorbed dose of ^{177}LuPSMA617 could be predicted in tumor lesions and organs at risk including kidneys, salivary glands and liver [6]. Although some previous studies showed the simultaneous imaging of other radionuclides like ^{99m}Tc and ^{18}F [10], [11], the activity of ^{68}Ga-DOTA-TATE from PET/CT images and the activity of ^{177}Lu-DOTA-TATE from SPECT/CT images were not obtained simultaneously in previous studies to have a better understanding of the pharmacokinetics in the same animal. In addition, the relationship between the uptake of ^{68}Ga-DOTA-TATE and ^{177}Lu-DOTA-TATE in normal organs has not been reported in previous studies.

In this study, we investigated the relationship between the uptake of ^{68}Ga-DOTA-TATE and ^{177}Lu-DOTA-TATE in organs and tumors when they are administered at the same time, and investigated a feasibility of using ^{68}Ga-DOTA-TATE image values to estimate the absorbed doses of ^{177}Lu-DOTA-TATE. We also showed the role of SSTR2 overexpression *in vivo* for ^{68}Ga-DOTA-TATE and ^{177}Lu-DOTA-TATE uptake.

II. MATERIALS AND METHODS

A. Animal studies and biokinetics

The Institute for Medical Research-32 (IMR32) cancer cell line [12], which belongs to the type of neuroblastic cancer, were implanted subcutaneously to the shoulders of three NOD SCID gamma (NSD) mice. In order to evaluate the role of SSTR2 overexpression, the IMR32 empty vector cells and the IMR32-SSTR2 (i.e., transduced to overexpress SSTR2) cells were implanted in each mouse. Hence, each mouse had two tumor xenografts, one of IMR32 in the right shoulder and the other of IMR32-SSTR2 in the left shoulder. After the sufficient growth of the tumors over 100 mm^3, approximately 11.8 MBq ^{68}Ga-DOTA-TATE and 11.1 MBq of ^{177}Lu-DOTA-TATE were mixed in approximately 0.1 ml aqueous solution and administered to each mouse via tail vein so that we could track them simultaneously. To investigate the *in vivo* biodistribution of these radiopharmaceuticals, each mouse was scanned by VECTor^{4}CT scanner (MILabs, Utrecht, The Netherlands) at five time points sequentially: about 0 hr, 4 hr, 24 hr, 48 hr and 96 hr postinjection. The scanner uses a thicker NaI detector and a collimator (HE-GP-RM) designed for high energy photons with the clustered multi-pinhole technology [10], [11], which is capable of imaging the photopeaks of both ^{177}Lu (208 keV) and ^{68}Ga (511 keV). 20% energy windows were used for both photopeaks and the automatic triple energy window technique was applied for scatter correction [13]. Each SPECT acquisition time was 1 hour and the projection data were reconstructed using the pixel-based ordered subset expectation maximization (POSEM) algorithm provided by the MILabs reconstruction software using 4 subsets for 50 iterations [14]. Each reconstructed SPECT image was filtered by a Gaussian kernel with a standard deviation of 1.5 mm and attenuation corrected based on the corresponding reconstructed CT image. The spatial resolution of the reconstructed SPECT image was about 2.4 mm based on the specification for the collimator used for this study, provided by the scanner manufacture. The reconstructed SPECT/CT images were co-registered in the volume of 400 × 400 × 2019 image voxels with a voxel size of 0.08 mm × 0.08 mm × 0.08 mm. We calibrated the SPECT scanner by imaging a mouse-sized cylinder phantom filled with a known activity concentration of ^{177}Lu and ^{68}Ga separately, and calculated the calibration factors of ^{177}Lu and ^{68}Ga to transform the corresponding reconstructed SPECT images in *Bq/ml*. For the reliability of the derived calibration factor, we repeated the derivation of the factor multiple times with the time span of a few months, and confirmed that the calibration factor was reproducible. Due to the short half-life of ^{68}Ga, the data for ^{68}Ga-DOTA-TATE were reconstructed only at 0 hr and 4 hr. All live animal procedures were approved by the local Institutional Animal Care and Use Committee prior to the study.

B. Absorbed dose calculation and estimation

Organ-based absorbed dose is defined as the total deposited energy in the target organ divided by the organ's mass. We calculate the absorbed dose D using Eq. 1 [15].

$$\begin{bmatrix} D_{t_1} \\ D_{t_2} \\ \vdots \\ D_{t_m} \end{bmatrix} = A_0 \times \begin{bmatrix} S_{t_1 \leftarrow s_1} & \cdots & S_{t_1 \leftarrow s_n} \\ S_{t_2 \leftarrow s_1} & \cdots & S_{t_2 \leftarrow s_n} \\ \vdots & \ddots & \vdots \\ S_{t_m \leftarrow s_1} & \cdots & S_{t_m \leftarrow s_n} \end{bmatrix} \times \begin{bmatrix} \tilde{a}_{s_1} \\ \tilde{a}_{s_2} \\ \vdots \\ \tilde{a}_{s_n} \end{bmatrix} \tag{1}$$

where $t_i (i = 1, ..., m)$ represents the target organ and $s_j (j = 1, ..., n)$ represents the source organ. The S-value $S_{t_i \leftarrow s_j}$ (unit: mGy/MBq·s) describes the absorbed dose rate to the target organ t_i per unit activity of a specific radionuclide in the source organ s_j. A_0 is the total initial injected activity and $\tilde{a}_{s_j}$ (unit: MBq·hr/MBq) is the time-integrated activity coefficient (TIAC) and analytically calculated as the integral of the normalized time-activity curve (TAC) (normalized by A_0) from 0 time point to infinity.

In this study, the segmented source organs were brain, heart, lungs, liver, stomach, kidneys, the tumor on the right shoulder (IMR32 or tumor1r), and the tumor on the left shoulder (IMR32-SSTR2 or tumor2l). For dose calculation, the source organs also included the remainder body, whose TIACs and S-values were calculated in Eq. 2 when the total body was regarded as the entire source.

$$\tilde{a}_{rb} = \tilde{a}_{tb} - \sum_j \tilde{a}_{s_j}, \qquad j = 1, ..., n, s_j \neq tb \tag{2}$$

$$S_{t_i \leftarrow rb} = \frac{m_{tb}}{m_{rb}} S_{t_i \leftarrow tb} - \sum_j \frac{m_{s_j}}{m_{rb}} S_{t_i \leftarrow s_j}$$

$$j = 1, ..., n, \qquad s_j \neq tb, \qquad i = 1, ..., m$$

where the subscript tb and rb represent total body and remainder body respectively, and m_{s_j} is the mass of the source organ s_j calculated based on the segmentation. Correspondingly, the target organs contained cranium, residual soft tissue (RST), and the segmented source organs. We first manually segmented the CT images of each mouse into the segmented source organs and determined the segmentation boundaries based on the reconstructed and co-registered SPECT and CT images. S-values of ^{177}Lu-DOTA-TATE were obtained using the voxelized Monte Carlo dosimetry simulations developed using Geant4 [15], which could serve as the prior knowledge for each mouse to calculate the absorbed dose of ^{177}Lu-DOTA-TATE in Eq. 1. The CT images of each mouse were loaded to Geant4 as the voxelized anatomical map by converting the Hounsfield unit (HU) in CT to organ materials in Geant4. Each source organ was treated as a 3D source map where the source particle ^{177}Lu ions with the complete decay chain were uniformly sampled. We used the

default electromagnetic standard physics list (G4EmStandardPhysics) together with the decay physics lists (G4DecayPhysics and G4RadioactiveDecayPhysics) in Geant4 with a default cut-off of 1.0 mm for the simulations. We ran the simulations on a dedicated Linux-based computing server for 10 times for each source organ and calculated the mean and the standard deviation of S-values. Since S-values are independent of the activity concentration of the source organs, we need to make sure that an adequate number of the source particle ^{177}Lu ions was simulated in the source organs to decrease the statistical uncertainty for S-values calculation. For each simulation, 1e6 ^{177}Lu particles were sampled from the source organs and 1e7 ^{177}Lu particles were sampled from the total body. The more particles we ran, the less uncertainties for S-values calculation. But it took more time and computation memory to run more ^{177}Lu particles in one simulation. We decreased the statistical uncertainty for S-values calculation by running each simulation for 10 times and we have checked that the relative standard deviations for the mean S-values were 1.59% ±1.54% for all of the three mice.

The flowchart of calculating and estimating the absorbed doses of ^{177}Lu-DOTA-TATE is shown in Figure 1. With the reconstructed SPECT images at the scanned time points, we obtained the total activity of ^{68}Ga-DOTA-TATE and ^{177}Lu-DOTA-TATE in the segmented source organs and the total body using the AMIDE software [16]. The physical-decay-corrected percent of injected activity (%IA) values in the segmented source organs and the total body were used to fit the biokinetics of ^{177}Lu-DOTA-TATE so that we only considered the biological retention of ^{177}Lu-DOTA-TATE. In many instances, the biokinetics is modeled as a sum of exponential functions $\%IA(t) = \sum_i a_i e^{-k_i t}$, where positive values for the fitting parameters a_i and k_i describe an uptake phase and negative a_i and k_i values describe an elimination phase [17]. In previous studies, the biexponential curve fitting was widely used to model the biokinetics as a fast and a slow clearance phase [15]. A more accurate biokinetics model used the tri-exponential curve fitting, representing an initial uptake phase and the following fast and slow clearance phases [18]. Though good fitting performance of the tri-exponential function [18], in this study we kept using the biexponential curve fitting for the following two reasons. One reason was that the first measurement for all three mice was taken at about 0.09 hr postinjection, indicating that the uptake of activity was happening very rapidly within a few minutes postinjection, and thus the uptake phase was negligible. The other reason was that there would be overfitting by using 6 data (5 measurement data and the initial 0 value at 0 time point) to estimate 6 unknown fitting parameters in the tri-exponential function. All of the fittings were performed using the nonlinear least squares solver in MATLAB. Fitting the %IA values of ^{177}Lu-DOTA-TATE with the biexponential function $\%IA(t) = a_1 e^{-k_1 t} + a_2 e^{-k_2 t}$ in the segmented source organs of each mouse, the TIACs of ^{177}Lu-DOTA-TATE were accounted for both biological retention and physical decay of ^{177}Lu-DOTA-TATE and calculated as $\tilde{a} = \frac{a_1}{k_1 + \lambda_{\text{Lu}-177}} + \frac{a_2}{k_2 + \lambda_{\text{Lu}-177}}$, where $\lambda_{\text{Lu}-177}$ is the physical decay constant of ^{177}Lu. Taking into account the excretion of ^{177}Lu-DOTA-TATE, the %IA values of excretion at the five time points, which equal to 1 minus the corresponding %IA values of total body, were fitted with an inverse-exponential function $\%IA_{exc} = a_1\left(1 - e^{-k_1 t}\right)$. Then the TIAC of ^{177}Lu-DOTA-TATE in the total body was

calculated as $\tilde{a}_{tb} = \frac{1 - a_1}{\lambda_{\text{Lu-177}}} + \frac{a_1}{k_1 + \lambda_{\text{Lu-177}}}$. Following Eq. 2, we then obtained the TIAC of ^{177}Lu-DOTA-TATE in the remainder body. Finally, the absorbed doses of ^{177}Lu-DOTA-TATE in the target organs were calculated using Eq. 1.

Given that ^{68}Ga has a shorter half-life than that of ^{177}Lu, the decay-corrected %IA values of ^{68}Ga-DOTA-TATE were obtained only at the two time points (0 hr and 4 hr). To estimate the absorbed doses of ^{177}Lu-DOTA-TATE, the challenge is how to use the %IA values of ^{68}Ga-DOTA-TATE at the two time points to estimate the TIACs of ^{177}Lu-DOTA-TATE. In this study, we tested various quantities that could be derived from the %IA values of ^{68}Ga-DOTA-TATE at the two time points, including the extrapolated clearance time (t_c), the extrapolated %IA value at strictly 0 hr (%IA(0)), the %IA value at 4 hr (%IA(4)), and the triangular areas of the %IA value-time line (*area*), trying to find some robust quantity to linearly correlate with the TIACs of ^{177}Lu-DOTA-TATE in the source organs. Especially we preferred to use the quantities from ^{68}Ga-DOTA-TATE in the total body to estimate the TIACs of ^{177}Lu-DOTA-TATE in the remainder body, eliminating the calculation of the TIACs of ^{177}Lu-DOTA-TATE in the total body. Three figures of merit (FOMs) were used to evaluate the linear least-squares regression performance, including R-squared (R^2) value, Pearson correlation coefficient (ρ) and the *p*-values.

III. RESULTS

A representative coronal slice of the reconstructed SPECT images overlaid on CT images of Mouse 1 at 4 hr is shown in Figure 2 (a). Masks of the segmented the source organs are shown in Figure 2 (b). The reconstructed activities of both ^{68}Ga-DOTA-TATE and ^{177}Lu-DOTA-TATE in the tumor2l are very heterogeneous in Figure 2.

The %IA values of ^{177}Lu-DOTA-TATE in the segmented source organs and the %IA values of excretion as a function of time are shown in Figure 3. We fitted the %IA values of ^{177}Lu-DOTA-TATE in the heart of Mouse 3 with the exponential decay function as shown in Figure 3 because the fast clearance phase was dominant in the heart of Mouse 3 and the R^2 value was 0.9999 when using one exponential decay function for fitting. When using the biexponential function for fitting in the heart of Mouse 3, the fitting parameters for the second exponential function were almost zeros no matter whether we assumed the second phase was an uptake phase (i.e. positive a_2 and k_2 values) or a clearance phase (i.e. negative a_2 and k_2 values), in addition to the fast clearance phase described by the first exponential function. Thus the contribution of the second exponential function to the TIAC of ^{177}Lu-DOTA-TATE in the heart of Mouse 3 was negligible. Given that the %IA values of ^{177}Lu-DOTA-TATE in the heart of Mouse 3 was low and had uncertainties, we used the exponential decay function to avoid overfitting.

The %IA values of ^{68}Ga-DOTA-TATE in the segmented source organs and the total body are shown in Figure 4. We used the quantities from the %IA values of ^{68}Ga-DOTA-TATE (t_c, %IA(0), %IA(4) and *area* shown in Figure 4) in the segmented source organs to estimate the TIAC of ^{177}Lu-DOTA-TATE in the same organ. In addition, we used quantities from the %IA values of ^{68}Ga-DOTA-TATE in the total body to estimate the TIAC of ^{177}Lu-DOTA-TATE in the remainder body.

The FOMs of fitting the quantities of the %IA values of ^{68}Ga-DOTA-TATE to the TIACs of ^{177}Lu-DOTA-TATE in the source organs are shown in Table I. Among all the quantities of the %IA values of ^{68}Ga-DOTA-TATE, we chose the quantities that were proportional to the TIACs of ^{177}Lu-DOTA-TATE with positive ρ and optimal or suboptimal fitting FOMs. We also preferred to minimize the number of selected quantities to robustly and easily estimate the TIACs of ^{177}Lu-DOTA-TATE. Based on these criteria, the extrapolated clearance time t_c and the extrapolated %IA value at 0 hr %$IA(0)$ provided the optimal or suboptimal fitting performance in the source organs (see Figure 5). Thus we used t_c of ^{68}Ga-DOTA-TATE to estimate the TIACs of ^{177}Lu-DOTA-TATE in the tumor2l, kidneys, brain, heart, liver, stomach and remainder body. We used %$IA(0)$ of ^{68}Ga-DOTA-TATE to estimate the TIACs of ^{177}Lu-DOTA-TATE in the tumor1r and lungs. Using both the calculated and estimated TIACs in the source organs of the three mice in Figure 5, we obtained the absorbed doses in the target organs for each mouse by Eq. 1 and the results are shown in Figure 6. The dotted line in Figure 6 shows when the absorbed doses of ^{177}Lu-DOTA-TATE in the target organs of the three mice calculated using the measurement of ^{177}Lu-DOTA-TATE are equal to the estimated doses calculated using the measurement of ^{68}Ga-DOTA-TATE. The absorbed dose ratios were calculated as the estimated doses of ^{177}Lu-DOTA-TATE calculated using the measurement of ^{68}Ga-DOTA-TATE divided by the referenced doses calculated using the measurement of ^{177}Lu-DOTA-TATE in the target organs. The mean and the standard deviation of the absorbed dose ratios of the three mice are shown in Table II.

Finally, we confirmed the obvious role of SSTR2 expression in uptake of both ^{68}Ga-DOTA-TATE and ^{177}Lu-DOTA-TATE. As evidenced in Figures 3 and 4, tumor2l (IMR32-SSTR2) showed much larger uptake in %IA than that in tumor1r (IMR32) in all three mice.

IV. Discussion

This study showed that we were able to image and track ^{68}Ga-DOTA-TATE and ^{177}Lu-DOTA-TATE simultaneously and quantitatively examine their biokinetics (see Figure 2). We also observed the role of SSTR2 *in vivo* in uptake levels of both ^{68}Ga-DOTA-TATE and ^{177}Lu-DOTA-TATE. Among all the source organs, ^{68}Ga-DOTA-TATE and ^{177}Lu-DOTA-TATE showed high uptake in kidneys, which makes kidneys as organs at risk in ^{177}Lu-DOTA-TATE therapy, as reported in clinical studies of ^{177}Lu-DOTA-TATE therapy [19]. Since the S-values were computed with homogeneous activity concentration simulated in Geant4, the heterogeneous activities of ^{177}Lu-DOTA-TATE in the tumor2l in Figure 2 would lead to either overestimating or underestimating the absorbed doses of ^{177}Lu-DOTA-TATE. If the activity of ^{177}Lu-DOTA-TATE is more concentrated in the center of tumor2l, the actual $S_{tumor2l \leftarrow tumor2l}$ value will be larger and thus we underestimate the absorbed dose of ^{177}Lu-DOTA-TATE in tumor2l, and vice versa.

The %IA values of ^{177}Lu-DOTA-TATE in Figure 3 and the %IA values of ^{68}Ga-DOTA-TATE in Figure 4 showed that the activity of ^{177}Lu and ^{68}Ga in the source organ would decrease rapidly in the first few hours postinjection due to biological elimination. The total activity at 4 hr was less than 50% of the activity at 0 hr in the source organs. The error of the measured total activity in the source organs was mainly caused by reconstruction and segmentation. The segmentation error could be estimated by making the segmentation

boundary of the source organs swell or diminish by a small distance and check the variation on the organ's total volume. Given that we manually segmented the source organs, the segmentation error due to human bias was not included in this preliminary study. For a more complete uncertainty estimation, one would need to investigate the errors coming from the iterative reconstruction algorithm in emission tomography, the influence of the inhomogeneous radiopharmaceutical absorption and the low counting statistics, which is beyond the scope of this study.

In Figure 5, the errors of the TIACs of ^{177}Lu-DOTA-TATE in the source organs of the three mice vary from organ to organ and mouse to mouse. The large errors of the TIACs in Figure 5 are mainly caused by the large relative standard deviations of the slower biological elimination factors (denoted as k_2 in Figure 5) when the fitted parameter values for k_2 are close to zero. It is challenging to find one quantity of the %IA values of ^{68}Ga-DOTA-TATE that can describe all source organs simultaneously and reliably. For tumor1r and lungs, $\%IA(0)$ of ^{68}Ga-DOTA-TATE is linearly correlated with the TIACs of ^{177}Lu-DOTA-TATE. For tumor2l, kidneys and the other source organs, t_c of ^{68}Ga-DOTA-TATE is linearly correlated with the TIACs of ^{177}Lu-DOTA-TATE based on the FOMs in Table I. However, this correlation is limited for statistical analysis due to the small number of enrolled mice and uncertainties in activity estimation in small regions. The image blurring caused by the motion of heart and lungs makes it difficult to properly segment and assign activity to. For liver and brain, all of the four quantities of the %IA values of ^{68}Ga-DOTA-TATE have good fitting results and t_c gives the best fitting FOMs. With the estimated TIACs of ^{177}Lu-DOTA-TATE, the estimated absorbed doses of ^{177}Lu-DOTA-TATE in the target organs of the three mice are close to the referenced absorbed doses calculated directly using ^{177}Lu-DOTA-TATE data per MBq of administered ^{177}Lu-DOTA-TATE, as shown in Figure 6 and Table II. The limited number of the enrolled mice degrades the statistical analysis and the predictive power in Table II. In Figure 6, it is worth noting that the absorbed doses of ^{177}Lu-DOTA-TATE in kidneys are highest among all target organs, which is expected and consistent with previous studies of ^{177}Lu-based therapy [6], [19]. ^{177}Lu-DOTA-TATE does contribute significant dose to the tumors as intended; however, the absorbed doses of ^{177}Lu-DOTA-TATE in lungs are comparable to those in the tumors because lungs have a much smaller density than other organs and thus a smaller mass, leading to a larger $S_{lungs \leftarrow lungs}$ value and a larger absorbed dose. Thus it shows that both kidneys and lungs are organs at risk in ^{177}Lu-DOTA-TATE therapy. Although the total activities of ^{177}Lu-DOTA-TATE in tumor2l are larger than those in tumor1r at all time points in Figure 3, the absorbed doses of ^{177}Lu-DOTA-TATE in tumor2l are not always larger than those in tumor1r in Figure 6. This may be true because the larger mass of tumor2l decreases the absorbed doses of ^{177}Lu-DOTA-TATE and the heterogeneous activities of ^{177}Lu-DOTA-TATE in the tumor2l in Figure 2, which are concentrated in the center of tumor2l, make the absorbed doses of ^{177}Lu-DOTA-TATE underestimated in areas of high uptake.

As a feasibility study, the small sample size is a limitation for the statistical analysis. Although we achieved $p < 0.05$ in the fitting between the TIAC of ^{177}Lu-DOTA-TATE and the extrapolated clearance time of ^{68}Ga-DOTA-TATE in the IMR32-SSTR2 tumor (i.e, tumor2l in Table I), the other organs showed a lower statistical significance ($p >$

0.05). However, R^2 values are over 0.9 for the IMR32-SSTR2 tumors, kidneys and lungs, which is important for predicting dose-dependent efficacy (tumors) and estimating radiation-dependent risk for organs at risk (kidneys and lungs). Our study is focused on the feasibility of this type of technique, and more importantly the utility of simultaneously imaging both ^{68}Ga-DOTA-TATE and ^{177}Lu-DOTA-TATE, which is the advantage of the technique. Simultaneous imaging of both SPECT and PET radionuclides is useful to investigate the pharmacokinetics in the same animal to develop theranostic pairs like ^{68}Ga-DOTA-TATE and ^{177}Lu-DOTA-TATE. One limitation of this technique is that we could not obtain many SPECT scans of ^{68}Ga-DOTA-TATE due to the short half-life of ^{68}Ga. It is hard to apply this technique in clinical applications without a SPECT scanner that is able to image both SPECT radionuclides like ^{177}Lu and PET radionuclides like ^{68}Ga. In conventional clinical acquisitions, people rely on both PET and SPECT imaging separately. However, as shown in our experiment that investigated biokinetics of both radiopharmaceuticals in the same animal and at the same time, for any question that can be performed appropriately using animal models, our technique will be useful.

V. CONCLUSION

In this work we investigated a technique of simultaneous imaging of ^{68}Ga-DOTA-TATE and ^{177}Lu-DOTA-TATE in mice, and showed the role of SSTR2 for *in vivo* uptake of these two radiopharmaceuticals in murine models of neuroblastoma. As a feasibility study, with measurements of ^{68}Ga-DOTA-TATE at the two time points to obtain the extrapolated clearance time t_c and the extrapolated %IA value at 0 hr %$IA(0)$, it was possible to predict the absorbed doses of ^{177}Lu-DOTA-TATE prospectively. The kidneys and lungs were found to be organs at risks in our murine study in ^{177}Lu-DOTA-TATE therapy. Since we only enrolled three mice in this study, it was limiting the statistical analysis and predicting power. Based on this investigation, a future study using a larger sample size would be warranted to further validate the correlation between ^{68}Ga-DOTA-TATE and ^{177}Lu-DOTA-TATE using the simultaneous imaging technique as shown in our study.

Acknowledgments

REFERENCES

[1]. Sackstein PE, O'Neil DS, Neugut AI, Chabot J, and Fojo T, "Epidemiologic trends in neuroendocrine tumors: an examination of incidence rates and survival of specific patient subgroups over the past 20 years," in Seminars in oncology, vol. 45, no. 4. Elsevier, 2018, pp. 249–258. [PubMed: 30348533]

[2]. Kennedy J, Chicheportiche A, and Keidar Z, "Quantitative SPECT/CT for dosimetry of peptide receptor radionuclide therapy," in Seminars in nuclear medicine, vol. 52, no. 2, pp. 229–242, 2022. [PubMed: 34911637]

[3]. Maris JM, "Recent advances in neuroblastoma," New England Journal of Medicine, vol. 362, no. 23, pp. 2202–2211, 2010. [PubMed: 20558371]

[4]. Zhang L, Vines DC, Scollard DA, McKee T, Komal T, Ganguly M, Do T, Wu B, Alexander N, Vali R. et al. , "Correlation of somatostatin receptor-2 expression with Gallium-68-DOTA-TATE uptake in neuroblastoma xenograft models," Contrast media & molecular imaging, vol. 2017, 2017.

[5]. Seo Y, Huh Y, Huang S.-y., Hernandez-Pampaloni JM, Hawkins RA, Gustafson WC, Vo KT, and Matthay KK, "Simplified and practical pretherapy tumor dosimetry—a feasibility study for 131I-MIBG therapy of neuroblastoma using 124I-MIBG PET/CT," Medical physics, vol. 46, no. 5, pp. 2477–2486, 2019. [PubMed: 30761545]

[6]. Peters S, Hofferber R, Privé BM, de Bakker M, Gotthardt M, Janssen M, de Lange F, Muselaers CH, Mehra N, Witjes JA et al. , "[68Ga] Ga-PSMA-11 pet imaging as a predictor for absorbed doses in organs at risk and small lesions in [177Lu] Lu-PSMA-617 treatment," European Journal of Nuclear Medicine and Molecular Imaging, pp. 1–12, 2021.

[7]. Kolbert KS, Pentlow KS, Pearson JR, Sheikh A, Finn RD, Humm JL, and Larson SM, "Prediction of absorbed dose to normal organs in thyroid cancer patients treated with 131I by use of 124I PET and 3-dimensional internal dosimetry software," Journal of Nuclear Medicine, vol. 48, no. 1, pp. 143–149, 2007. [PubMed: 17204711]

[8]. Kim Y.-i., Oh J, Yoo C, Ryoo B-Y, and Ryu J-S, "Prediction of absorbed dose by tumors and critical organs after Lu-177-DOTATATE therapy using pretherapeutic Ga-68-DOTATOC PET/ CT," 2021.

[9]. Ortega C, Wong RK, Schaefferkoetter J, Veit-Haibach P, Myrehaug S, Juergens R, Laidley D, Anconina R, Liu A, and Metser U, "Quantitative 68Ga-DOTATATE PET/CT parameters for the prediction of therapy response in patients with progressive metastatic neuroendocrine tumors treated with 177Lu-DOTATATE," Journal of Nuclear Medicine, vol. 62, no. 10, pp. 1406–1414, 2021. [PubMed: 33579805]

[10]. Goorden MC and Beekman FJ, "High-resolution tomography of positron emitters with clustered pinhole SPECT," Physics in Medicine & Biology, vol. 55, no. 5, p. 1265, 2010. [PubMed: 20134086]

[11]. Miwa K, Inubushi M, Takeuchi Y, Katafuchi T, Koizumi M, Saga T, and Sasaki M, "Performance characteristics of a novel clustered multi-pinhole technology for simultaneous high-resolution SPECT/PET," Annals of nuclear medicine, vol. 29, no. 5, pp. 460–466, 2015. [PubMed: 25894055]

[12]. Tumilowicz JJ, Nichols WW, Cholon JJ, and Greene AE, "Definition of a continuous human cell line derived from neuroblastoma," Cancer research, vol. 30, no. 8, pp. 2110–2118, 1970. [PubMed: 5459762]

[13]. Shao L, Freifelder R, and Karp JS, "Triple energy window scatter correction technique in PET," IEEE transactions on medical imaging, vol. 13, no. 4, pp. 641–648, 1994. [PubMed: 18218542]

[14]. Branderhorst W, Vastenhouw B, and Beekman FJ, "Pixel-based subsets for rapid multi-pinhole SPECT reconstruction," Physics in Medicine & Biology, vol. 55, no. 7, p. 2023, 2010. [PubMed: 20299722]

[15]. Huang S.-y, Bolch WE, Lee C, Van Brocklin HF, Pampaloni MH, Hawkins RA, Sznewajs A, DuBois SG, Matthay KK, and Seo Y, "Patient-specific dosimetry using pretherapy [124 I] miodobenzylguanidine ([124 I] mIBG) dynamic PET/CT imaging before [131 I] mIBG targeted radionuclide therapy for neuroblastoma," Molecular imaging and biology, vol. 17, no. 2, pp. 284–294, 2015. [PubMed: 25145966]

[16]. Loening AM and Gambhir SS, "AMIDE: a free software tool for multimodality medical image analysis," Molecular imaging, vol. 2, no. 3, p. 15353500200303133, 2003.

[17]. Stabin MG, Fundamentals of nuclear medicine dosimetry. Springer Science & Business Media, 2008.

[18]. Jackson P, McIntosh L, Hofman MS, Kong G, and Hicks RJ, "Rapid multiexponential curve fitting algorithm for voxel-based targeted radionuclide dosimetry," Medical Physics, vol. 47, no. 9, pp. 4332–4339, 2020. [PubMed: 32426853]

[19]. Seregni E, Maccauro M, Chiesa C, Mariani L, Pascali C, Mazzaferro V, De Braud F, Buzzoni R, Milione M, Lorenzoni A. et al. , "Treatment with tandem [90 Y] DOTA-TATE and [177 Lu] DOTA-TATE of neuroendocrine tumours refractory to conventional therapy," European journal of nuclear medicine and molecular imaging, vol. 41, no. 2, pp. 223–230, 2014. [PubMed: 24233003]
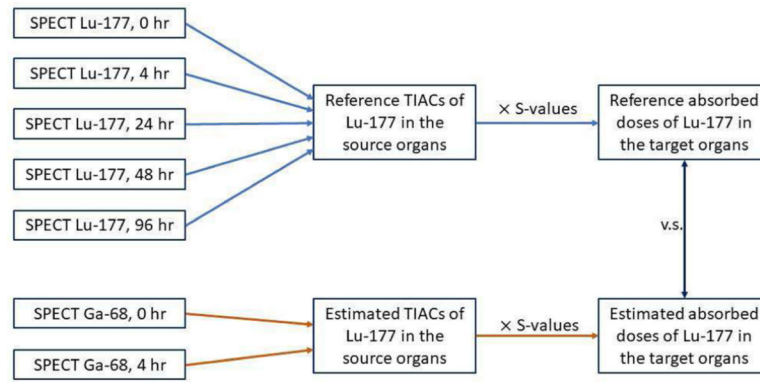
Fig. 1.
The flowchart of calculating and estimating absorbed doses of ^{177}Lu-DOTA-TATE.
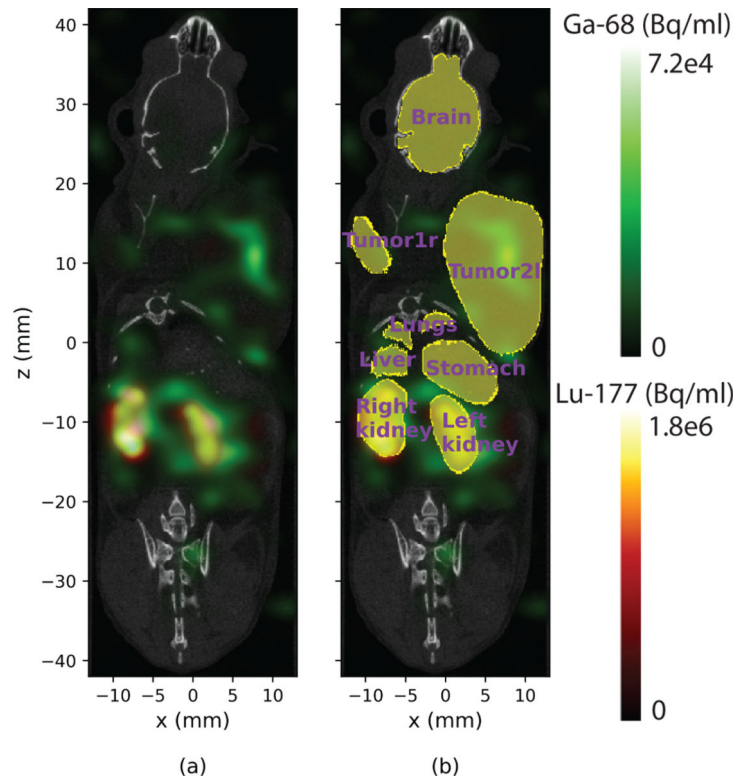
Fig. 2.
(a) A coronal slice of the reconstructed CT image, SPECT image of ^{68}Ga-DOTA-TATE (shown in green colormap) and SPECT image of ^{177}Lu-DOTA-TATE (shown in hot iron colormap) of Mouse 1 at 4 hr postinjection. Each voxel is 0.08 mm × 0.08 mm × 0.08 mm. (b) The segmentation of (a).
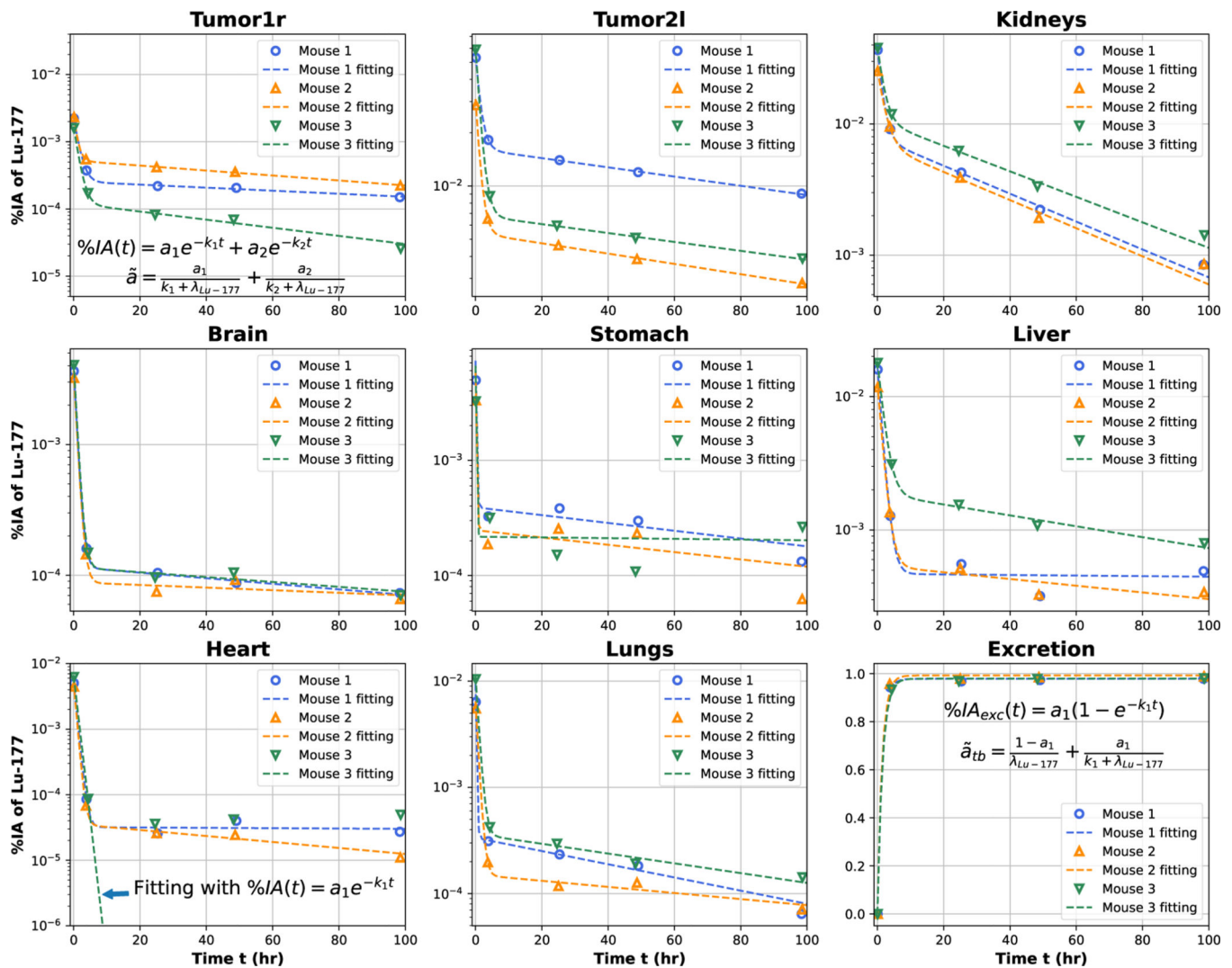
Fig. 3.
The %IA values of ^{177}Lu-DOTA-TATE in the segmented source organs and the %IA values of excretion at the five measurement time points. We fitted the segmented source organs with the biexponential function (and the exponential decay function for the heart of Mouse 3) and fitted excretion with the inverse-exponential function to obtain $\tilde{a}$, the TIACs of ^{177}Lu-DOTA-TATE.
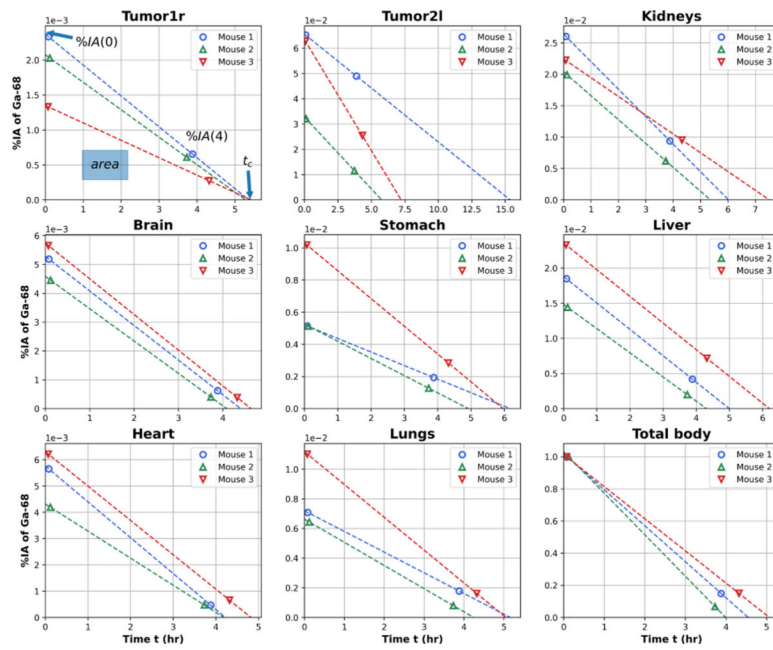
Fig. 4.
The %IA values of ^{68}Ga-DOTA-TATE in the segmented source organs and the total body at the two measurement time points.
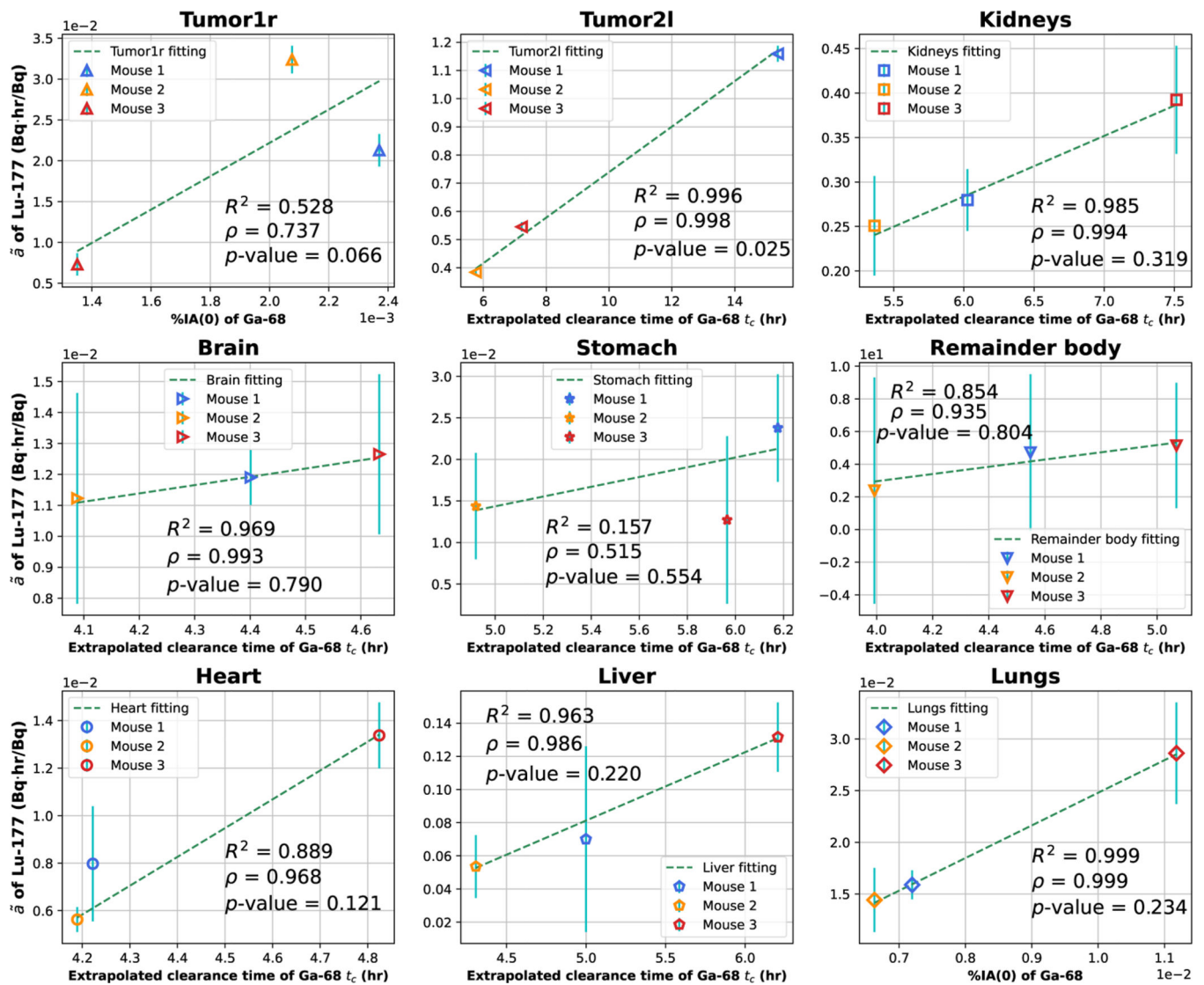
Fig. 5.

Fitting from the quantities of the %IA values of ^{68}Ga-DOTA-TATE to the TIACs of ^{177}Lu-DOTA-TATE in the source organs of the three mice. The extrapolated clearance time t_c gave the best fitting in tumor2l, kidneys, brain, stomach, heart, liver and the remainder body. The extrapolated %IA value at 0 hr %IA(0) gives the best fitting in tumor1r and lungs. The errors of the TIACs of ^{177}Lu-DOTA-TATE came from the errors of the fitting parameter when calculating the TIACs in Figure 3.

Fig. 6.
The absorbed doses of ^{177}Lu-DOTA-TATE in the target organs in the three mice. The x-axis is the referenced dose calculated using the measurement of ^{177}Lu-DOTA-TATE, and the y-axis shows the estimated dose calculated using the measurement of ^{68}Ga-DOTA-TATE. The unit of the absorbed dose is mGy per MBq of injected ^{177}Lu-DOTA-TATE.
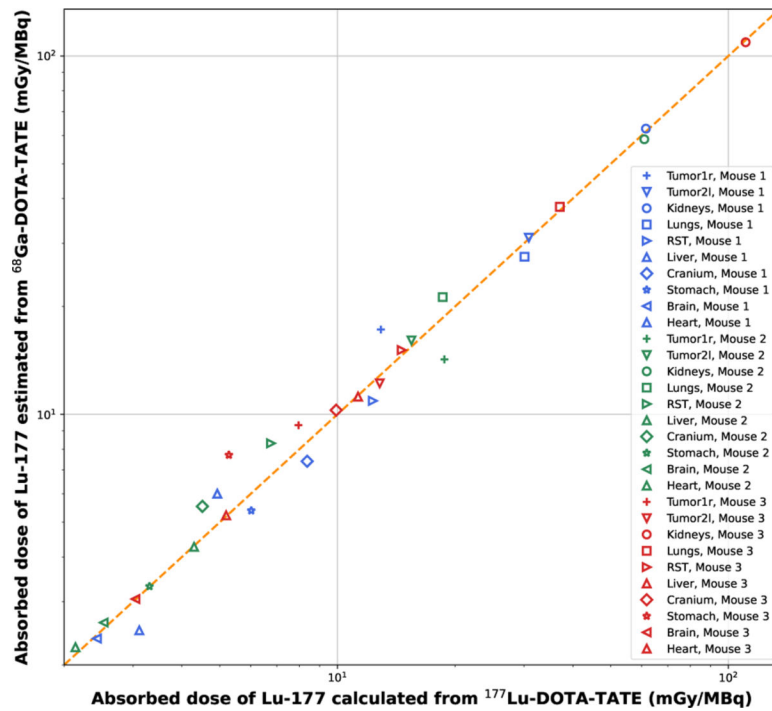
TABLE I

FOMs OF FITTING THE QUANTITIES OF THE %IA VALUES OF ^{68}Ga-DOTA-TATE TO THE TIACs OF ^{177}Lu-DOTA-TATE.

Organs	FOMs	t_c	%/IA(0)	%/IA(4)	area
Tumor1r	R^2	0.970	0.528	0.397	0.486
	ρ	−0.986	0.737	0.648	0.710
	ρ	0.055	0.066	0.073	0.068
Tumor21	R^2	0.996	0.359	0.879	0.977
	ρ	0.998	0.703	0.956	0.992
	ρ	0.025	0.035	0.027	0.025
Kidneys	R^2	0.985	−0.039	0.643	0.462
	ρ	0.994	0.014	0.853	0.764
	ρ	0.319	0.870	0.398	0.456
Brain	R^2	0.969	0.952	0.978	0.971
	ρ	0.993	0.989	0.995	0.994
	ρ	0.790	0.792	0.789	0.789
Heart	R^2	0.889	0.739	0.943	0.932
	ρ	0.968	0.887	0.982	0.973
	ρ	0.121	0.123	0.121	0.121
Lungs	R^2	−0.205	0.999	0.302	0.898
	ρ	0.488	0.999	0.834	0.975
	ρ	0.696	0.234	0.369	0.253
Liver	R^2	0.963	0.905	0.960	0.962
	ρ	0.986	0.964	0.985	0.986
	ρ	0.220	0.221	0.220	0.220
Stomach	R^2	0.157	0.387	−0.021	0.199
	ρ	0.515	−0.622	−0.303	−0.477
	ρ	0.554	0.664	0.982	0.804
Remainder body	R^2	0.854	0.993	0.905	0.841
	ρ	0.935	−0.997	0.958	0.929
	ρ	0.804	0.787	0.798	0.806

TABLE II

The absorbed dose ratios of ^{177}Lu-DOTA-TATE in the target organs. The ratio is defined as the estimated dose calculated using the measurement of ^{68}Ga-DOTA-TATE divided by the referenced dose calculated using the measurement of ^{177}Lu-DOTA-TATE.

Organs	Absorbed dose ratios
Tumor1r	1.09 ± 0.24
Tumor21	1.00 ± 0.04
Kidneys	0.99 ± 0.02
Lungs	1.02 ± 0.09
RST	1.05 ± 0.14
Liver	1.07 ± 0.11
Cranium	1.05 ± 0.14
Stomach	1.12 ± 0.24
Brain	1.02 ± 0.02
Heart	0.95 ± 0.10